

# Gauge-Quintessence

**A. Mehrabi<sup>a,c</sup> A. Maleknejad<sup>b</sup> and V. Kamali,<sup>a,b</sup>**

<sup>a</sup>Department of Physics, Bu-Ali Sina University, Hamedan 65178, 016016, Iran

<sup>b</sup>School of Physics, Institute for Research in Fundamental Sciences (IPM),  
P. Code. 19538-33511, Tehran, Iran

<sup>c</sup>School of Astronomy, Institute for Research in Fundamental Sciences (IPM),  
P. O. Box 19395-5746, Tehran, Iran

E-mail: [Mehrabi@basu.ac.ir](mailto:Mehrabi@basu.ac.ir), [azade@ipm.ir](mailto:azade@ipm.ir), [vkamali@basu.ac.ir](mailto:vkamali@basu.ac.ir)

**Abstract.** In this work, we introduce a new quintessence model associated with non-Abelian gauge fields, minimally coupled to Einstein gravity. This gauge theory has been originally introduced and studied as an inflationary model, called gauge-flation. Here, however, we are interested in the late time cosmology of the model in the presence of matter and radiation to explain the present time accelerating Universe. During the radiation and matter eras, the gauge field tracks radiation and basically acts like a dark radiation sector. As we approach lower redshifts, the dark component takes the form of a dark energy source which eventually becomes the dominate part of the energy budget of the Universe. Due to the tracking feature of our model, solutions with different initial values are attracted to a common trajectory. The existence of early dark radiation is a robust prediction of our model which contributes to the effective number of relativistic species,  $N_{\text{eff}}$  and has its own interesting observational features.

---

## Contents

<b>1</b>	<b>Introduction</b>	<b>1</b>
<b>2</b>	<b>Gauge-Quintessence model</b>	<b>3</b>
2.1	Background evolution	3
<b>3</b>	<b>Cosmological evolution, analytical treatment</b>	<b>4</b>
3.1	Matter dominated epoch	5
3.2	Dark energy dominated epoch	6
<b>4</b>	<b>Late time accelerated expansion, numerical analysis</b>	<b>6</b>
4.1	Generic features of the gauge-quintessence trajectories	8
<b>5</b>	<b>Contact with observational constraints</b>	<b>9</b>
5.1	Supernovae and BAO	9
5.2	Dark energy density at early times	11
5.3	Taylor expansion of $w$	13
<b>6</b>	<b>A quick treatment of the perturbations</b>	<b>14</b>
6.1	Anisotropic stress	14
6.2	Cosmic structure formation and the dark sector	14
<b>7</b>	<b>Discussion and Conclusions</b>	<b>15</b>

---

## 1 Introduction

The late time cosmic acceleration first confirmed by supernovae Ia (SnIa) surveys [1–3]. Moreover, other observations including large scale structure (LSS) [4, 5], cosmic microwave background (CMB) [6–8] and baryon acoustic oscillations (BAO) [9, 10] measurements indicate that about 70% of the energy density of the Universe today consists of an unknown component called dark energy (DE). The quest for the nature of DE is one of the most exciting challenges of the modern cosmology. Various observational projects are planned or envisioned to shed light on the physics underlying the observed cosmic acceleration and in the near future, we expect a wealth of new high quality data on that direction [11, 12].

The cosmological constant with equation of state  $w \equiv \frac{P_{DE}}{\rho_{DE}} = -1$  seems the most simple explanation for the late time accelerated expansion. However, if the cosmological constant is responsible for the current epoch of acceleration, its value ( $\Lambda \sim 10^{-120} M_{\text{pl}}^4$ ) is many orders of magnitude smaller than the theoretically expected value [13, 14]. Given the fact that the cosmological constant makes difficulties in any theoretical interpretation, it seems plausible to have a DE sector beyond the standard  $\Lambda$ CDM. It could be an unknown energy component in the universe, dark energy [15–19], or the modification of gravity as described by Einstein’s general relativity, modified gravity (MG) [20–23]. Those models lead to a similar late time expansion history as the cosmological constant with a much richer phenomenology [23–25].

Many of the dark energy and modified gravity models can be described by adding a scalar degree of freedom to Einstein gravity [26]. From the former viewpoint, one possibility is a canonical scalar field which varies slowly along its potential, known as the standard

quintessence model [19, 27, 28] with the possibility of link to the models of particle physics. On the other hand, dynamical gauge fields abound in models of particle physics, string theory, GUTs and etc. It is therefore natural to ask whether gauge fields can be involved in the new physics beyond vanilla  $\Lambda$ CDM, responsible for the present dark energy era. Inspired by that idea, one may explore the possibility of using non-Abelian gauge fields as a dark energy candidate.

Over the past decade, there have been interesting discussions in the literature of using non-Abelian gauge fields in inflationary models [29–32], models of dark energy [33, 34] and dark matter [35–37]. For a detailed review of literature on the gauge fields in inflation, see [38]. The interest in non-Abelian gauge fields is due to the fact that for a generic gauge invariant field theory, there is an isotropic and homogeneous field configuration for the  $SU(2)$  gauge field [29, 33]. In particular, choosing the temporal gauge  $A_0^a = 0$ , we can identify the  $SU(2)$  gauge index with the spatial rotation  $SO(3)$  index in the spatial elements of the field. The possibility of that identification then leads to an isotropic and homogeneous background solution of the form  $A_i^a = \phi(t)\delta_i^a$ . The next generic feature of gauge field models is that if the theory consists of *only* the Yang-Mills term, then the gauge field will track the radiation and damps like  $a^{-4}$  by the expansion of the Universe. In order to prevent that, one should break the conformal symmetry by coupling the gauge field to the other fields, e.g. Higgs boson [34] and axion field [39, 40], or adding new gauge invariant terms to the gauge field theory [29].

Among the interesting predictions of models including gauge fields is the existence of a weakly interacting dark radiation at high redshifts. Presence of additional relativistic degrees of freedom leads to important modifications comparing to the  $\Lambda$ CDM, e.g. changing the Hubble parameter and observable signals in the CMB [41, 42]. The observational measurements ( $N_{\text{eff}} = 3.15 \pm 0.23$ ) have been used to constrain the effective value of extra relativist degrees of freedom, with the current bound  $\Delta N_{\text{eff}} = 0.1 \pm 0.23$  [8]. On the theoretical point of view, most of inflationary and dark matter models motivated by string theory and particle physics beyond SM predict a form of dark radiation [35, 42, 43]. Future CMB polarization experiments will improve our constraints on these new physics by one or two order of magnitude [44]. This significant improvement in sensitivity of the future observational measurement, further fueled the interest in dark radiation.

In the present paper, we introduce a new quintessence model associated with non-Abelian gauge fields, *gauge-quintessence*. Our gauge field theory has been first presented and investigated as an inflationary model (gauge-flation) in which inflation is driven by non-Abelian gauge fields [29, 30]. Here, we are interested in the late time cosmology of the model in the presence of matter and to explore if this model can explain the present time accelerating Universe. Our gauge field theory consists of the Yang-Mills which acts like a dark radiation term and  $\kappa(F\tilde{F})^2$  with the equation of a state  $w = -1$ . Our model is parametrized by only two parameters, the gauge field coupling  $g$  and the dimensionfull prefactor  $\kappa$ . We are working on weakly coupled theories, thus, confinement in the dark sector is irrelevant.

This paper is organized as follows. In section 2, we introduce the setup of the gauge-quintessence model. We study the cosmological evolution of the model analytically in section 3. Section 4 studies the late time cosmology of the model and presents the result of numerical analysis of the DE trajectories. In section 5, we confront the model with the observational data and show the  $1\sigma$  and  $2\sigma$  confidence regions of the model parameters. Section 6 is devoted to the qualitative study of the cosmic perturbation in our model. Finally we conclude in section 7. Throughout this paper, we set the reduced Planck mass  $M_{pl}^2 = (8\pi G)^{-1}$ , equal to one.

## 2 Gauge-Quintessence model

The Gauge-Quintessence model consists of radiation, baryonic and cold dark matter (CDM), as well as a dark non-Abelian gauge field sector. The hidden gauge field sector is minimally coupled to Einstein gravity and interacts gravitationally with the visible matter. This model is specified by the following action

$$S = \int \sqrt{-g} \left( -\frac{1}{2}R - \frac{1}{4}(F_{\mu\nu}^a F_a^{\mu\nu} + \frac{\kappa}{24}(F_{\mu\nu}^a \tilde{F}^{a\lambda\sigma})^2) \right) d^4x + S_m(\chi_i, g_{\mu\nu}), \quad (2.1)$$

where  $R$  is the Ricci scalar,  $\tilde{F}^{a\mu\nu} = \frac{1}{2}\epsilon^{\mu\nu\lambda\sigma}F_{\lambda\sigma}^a$  and  $S_m$  is the matter action, including cold dark matter, baryons, photons and neutrinos. The *gauge-quintessence* action consists of the Yang-Mills and the  $(F\tilde{F})^2$  term and has two parameters  $\kappa$  and  $g$ . The gauge field strength  $F_{\mu\nu}^a$  is

$$F_{\mu\nu}^a = \partial_\mu A_\nu^a - \partial_\nu A_\mu^a - g\epsilon_{bc}^a A_\mu^b A_\nu^c, \quad (2.2)$$

where  $\epsilon_{abc}$  is the totally antisymmetric tensor,  $g$  is the gauge coupling and  $A_\mu^a$  is a 4-dimensional SU(2) gauge field. Note that here  $\mu, \nu, \dots$  and  $a, b, \dots$  are respectively used for the indices of the space-time and the gauge algebra. The gauge field theory  $\mathcal{L}_G$  has been originally introduced and investigated as an inflationary model in [29, 30], *gauge-flation* model. Here, on the other hand, we are interested in its late time evolution and whether it gives rise to the late time cosmic acceleration as a quintessence model. For discussion on the theoretical motivation for the model, see [30, 38].

For later convenience, it is useful to decompose the energy and the pressure density of the gauge field theory into dark radiation (DR) and dark energy (DE) parts

$$\rho_G = \rho_{DR} + \rho_{DE} \quad \text{and} \quad P_G = \frac{1}{3}\rho_{DR} - \rho_{DE}, \quad (2.3)$$

where  $\rho_{DE}$  and  $\rho_{DR}$  are the contributions of  $(F\tilde{F})^2$  and Yang-Mills terms respectively. In fact, DR is the contribution of the Yang-Mills, while the  $(F\tilde{F})^2$  is effectively the dark energy (DE) sector. Thus, the hidden gauge field has a time dependent equation of state

$$w(t) = \frac{\frac{1}{3}\rho_{DR} - \rho_{DE}}{\rho_{DR} + \rho_{DE}}. \quad (2.4)$$

Thus in the regime that  $\rho_{DE} \gg \rho_{DR}$ , the gauge sector is effectively a dark energy element. Note that EoS is bounded in the range  $-1 < w(t) < \frac{1}{3}$  and it never crosses the phantom line.

### 2.1 Background evolution

We now turn to investigate the background trajectories of the gauge-quintessence model. Considering the flat, isotropic and homogeneous FLRW metric

$$ds^2 = -dt^2 + a(t)^2 \delta_{ij} dx^i dx^j, \quad (2.5)$$

we have radiation and matter energy densities in terms of their energy density at the present time as  $\rho_r(t) = \frac{\rho_r^0}{a^4}$  and  $\rho_m(t) = \frac{\rho_m^0}{a^3}$ . To understand the dynamics of the gauge field sector, however, we need to solve the field equation for the isotropic and homogeneous space-time. The non-Abelian gauge field has the following isotropic and homogeneous configuration [29, 30]

$$A_0^a = 0 \quad \text{and} \quad A_i^a = \phi(t)\delta_i^a, \quad (2.6)$$

where  $i, j = 1, 2, 3$  are labels of spatial directions. For a more comprehensive detailed discussion on the above ansatz see [38]. Using field configuration 2.6 and FLRW metric 2.5, one can find the isotropic and homogeneous strength tensor

$$F_{0i}^a = \dot{\phi} \delta_i^a \quad \text{and} \quad F_{ij}^a = -g \phi^2 \epsilon_{ij}^a. \quad (2.7)$$

Moreover, the reduced action of the dark gauge field theory is

$$\mathcal{L}_G = \frac{3}{2} \left( \frac{\dot{\phi}^2}{a^2} - \frac{g^2 \phi^4}{a^4} + \kappa g^2 \frac{\dot{\phi}^2 \phi^4}{a^6} \right), \quad (2.8)$$

while the field equation of the gauge field ( $D_\mu (\frac{\delta \mathcal{L}}{\delta F_{\mu\nu}}) = 0$ ) can be determined as

$$(1 + \kappa g^2 \frac{\phi^4}{a^4}) \frac{\ddot{\phi}}{a} + (1 + \kappa \frac{\dot{\phi}^2}{a^2}) \frac{2g^2 \phi^3}{a^3} + (1 - 3\kappa g^2 \frac{\phi^4}{a^4}) \frac{H \dot{\phi}}{a} = 0. \quad (2.9)$$

Recalling (2.3), the energy density of the gauge field can be read as  $\rho_G = \rho_{DR} + \rho_{DE}$ , in which

$$\rho_{DE} = \frac{3}{2} \kappa \frac{g^2 \dot{\phi}^2 \phi^4}{a^6} \quad \text{and} \quad \rho_{DR} = \frac{3}{2} \left( \frac{\dot{\phi}^2}{a^2} + \frac{g^2 \phi^4}{a^4} \right). \quad (2.10)$$

In the presence of matter and radiation in a spatially flat universe, the Friedmann equations are

$$3 \left( \frac{\dot{a}}{a} \right)^2 = (\rho_m + \rho_r + \rho_{DR} + \rho_{DE}), \quad (2.11a)$$

$$3 \left( \frac{\ddot{a}}{a} \right) = - \left( \frac{1}{2} \rho_m + \rho_r + \rho_{DR} - \rho_{DE} \right). \quad (2.11b)$$

Working out the field equations, now we turn to the further study of the gauge-quintessence model during the matter and dark energy epochs.

### 3 Cosmological evolution, analytical treatment

Since we are not able to measure distance directly, but redshift, it is more convenient to rewrite the fields in terms of redshift  $z$  ( $a = \frac{1}{1+z}$ ). Here, for further simplification, we define the following dimensionless parameters

$$\tilde{g} = \frac{g}{H_0}, \quad \tilde{\kappa} = g^2 \kappa, \quad \text{and} \quad \tilde{t} = H_0 t, \quad (3.1)$$

where  $H_0$  is the present value of the Hubble constant [8]

$$H_0 = (67.8 \pm 0.9) \text{kms}^{-1} \text{Mpc}^{-1}, \quad (3.2)$$

which is  $H_0 \simeq 10^{-60} M_{pl}$ . Moreover, the energy density parameter of the gauge field,  $\Omega_G(z)$ , is defined as

$$\Omega_G(z) \equiv \frac{\rho_G}{\rho_c} = \Omega_{DR}(z) + \Omega_{DE}(z) \quad \text{where} \quad \rho_c = 3H_0^2, \quad (3.3)$$

where  $\Omega_{DR}(z)$  and  $\Omega_{DE}(z)$  are respectively the contributions of the dark radiation and dark energy sectors

$$\Omega_{DR}(z) = \frac{1}{2} \left( \phi'^2 (1+z)^2 + \tilde{g}^2 \phi^4 (1+z)^4 \right) \quad \text{and} \quad \Omega_{DE}(z) = \frac{1}{2} \left( \tilde{\kappa} \phi^4 \phi'^2 (1+z)^6 \right), \quad (3.4)$$

where “ $'$ ” means a derivative with respect to  $\tilde{t}$ . Using (3.1) and (3.4), we can rewrite the Friedmann equations (2.11), as

$$\left(\frac{z'}{1+z}\right)^2 = \Omega_{\text{DE}}(z) + \Omega_{\text{DR}}(z) + \Omega_{\text{m}}^0(1+z)^3 + \Omega_{\text{r}}^0(1+z)^4, \quad (3.5a)$$

$$\frac{z''}{1+z} = 3\left(\frac{z'}{1+z}\right)^2 - \frac{1}{2}\Omega_{\text{m}}^0(1+z)^3 - 2\Omega_{\text{DE}}(z), \quad (3.5b)$$

as well as the field equation of  $\phi$  (2.9) which is

$$(1 + \tilde{\kappa}\phi^4(1+z)^4)\phi'' + 2\tilde{g}^2\phi^3(1+z)^2 + 2\tilde{\kappa}\phi^3\phi'^2(1+z)^4 - (1 - 3\tilde{\kappa}\phi^4(1+z)^4)\frac{z'}{1+z}\phi' = 0, \quad (3.6)$$

where  $\Omega_x^0$  are the present-day density parameters. Given the fact that  $z(\tilde{t}_0) = 0$  and  $\sum_i \Omega_i(\tilde{t}_0) = 1$  (for a flat universe<sup>1</sup>), one can read  $\phi'(\tilde{t}_0)$  from (3.5a) as

$$\phi'(\tilde{t}_0) = \pm \sqrt{\frac{2(1 - \Omega_{\text{m}}^0 - \Omega_{\text{r}}^0) - \tilde{g}^2\phi_0^4}{(1 + \tilde{\kappa}\phi_0^4)}}. \quad (3.7)$$

Moreover, to ensure the flatness of the Universe, we require that

$$\Omega_G^0 = 1 - \Omega_{\text{r}}^0 - \Omega_{\text{m}}^0, \quad (3.8)$$

which after fixing the values of the parameters to the observational best values  $\Omega_{\text{m}}^0 = 0.308 \pm 0.012$  and  $\Omega_{\text{r}}^0 \sim 10^{-4}$ , gives  $\Omega_G^0 = 0.69$  [8]. Our gauge-quintessence model has three free parameters  $\tilde{\kappa}$ ,  $\tilde{g}$  and  $\phi_0$  as well as the sign of  $\phi'_0$ .

From the combination of (3.4) and (3.5b), we obtain

$$\frac{z''}{1+z} = 3\left(\frac{z'}{1+z}\right)^2 \left(1 - \frac{\tilde{\kappa}}{9}((1+z)^4(\phi^3)_z)^2\right) - \frac{1}{2}\Omega_{\text{m}}^0(1+z)^3, \quad (3.9)$$

in which the subscript “ $z$ ” denotes a derivative with respect to  $z$ . While numerical analysis is necessary to find the exact predictions of the model, yet approximate analytical solutions are possible in some limits. In the following, we integrate the above equations analytically for the matter and dark energy epochs and determine the form of  $\phi(z)$ . Later, on the next section, we report the result of full numerical study of the model.

### 3.1 Matter dominated epoch

During the matter domination, the scale factor is given as  $a(t) \propto \tilde{t}^{\frac{2}{3}}$  which implies that  $z \propto \tilde{t}^{-\frac{2}{3}}$ . Inserting  $z'(z) \simeq -(\Omega_{\text{m}}^0)^{\frac{1}{2}}(1+z)^{\frac{5}{2}}$  in (3.9), we obtain this relation for matter era

$$\frac{\tilde{\kappa}}{9}((1+z)^4(\phi^3)_z)^2 \ll 1.$$

Recalling the fact that  $\tilde{\kappa} \gg 1$ , the above relation implies that during the matter dominated epoch  $\phi(z)$  is a slow varying function of  $z$ , *i.e.*  $\phi_z(z) \ll 1$ . As the system evolves to lower redshifts during the matter dominated era, then  $\phi_z$  gradually increases by time. Note that

---

<sup>1</sup>Due to the restrictive observational upper bound on the value of the spatial curvature density parameter  $\Omega_K < 0.005$  [8], here, we assume that the background geometry is spatially flat.

the value of  $\phi_z$  is related to the value of  $\tilde{\kappa}$  and it decreases by increasing  $\tilde{\kappa}$ . Since  $\phi_z \ll 1$ , the density parameters are approximately

$$\Omega_{DR}(z) \simeq \frac{1}{2}\tilde{g}^2\phi^4(1+z)^4, \quad \text{and} \quad \Omega_{DE}(z) \simeq \frac{\tilde{\kappa}}{\tilde{g}^2}\phi_z^2 z'^2(1+z)^2\Omega_{DR}(z). \quad (3.10)$$

As  $\phi_z(z)$  increases by time evolution, one expect that the ratio of  $\frac{\Omega_{DE}}{\Omega_{DR}}$  increases as we are approaching the late times. After solving the field equation of  $\phi$  full numerically in the next section, we show that  $\Omega_{DR}(z) \gg \Omega_{DE}(z)$  at high redshifts. Hence the gauge field sector effectively acts like a dark radiation at  $z \gtrsim 5$  and evolves as  $\Omega_G(z) \simeq \Omega_{DR}(z) \propto a^{-4}$  (see Fig. 2).

### 3.2 Dark energy dominated epoch

At the late time dark energy dominated era and in the small redshift limit  $z \lesssim 0.1$ , the dark energy density parameter  $\Omega_{DE}(z)$  is a very slow varying function of  $z$ , *i.e.*  $\Omega_{DE}(z) \simeq 1 - \Omega_m^0$ . Using the fact that  $\Omega_r^0 \ll 1$ ,  $z'(\tilde{t}_0) = -1$ , combining equations (3.8) and (3.4), we obtain the following differential equation for  $\phi$  during the dark energy era

$$(\phi^3)_z \simeq \pm \left( \frac{6(1 - \Omega_m^0)}{\tilde{\kappa}} \right)^{\frac{1}{2}}, \quad (3.11)$$

up to the dominate order. Integrating the above equation, one can then find  $\phi(z)$

$$\phi(z) \simeq \phi_0 \left( 1 \pm \frac{6^{\frac{1}{2}}(1 - \Omega_m^0)^{\frac{1}{2}}}{\tilde{\kappa}^{\frac{1}{2}}\phi_0^3} z \right)^{\frac{1}{3}}, \quad (3.12)$$

which implies that in the very late time,  $\phi$  smoothly increases (decreases) by the redshift, depends on the sign of  $\phi'(\tilde{t}_0)$ . The late time value of redshift derivative of the gauge field is related to  $\tilde{\kappa}$ , while larger  $\tilde{\kappa}$ s lead to smaller  $\phi_z(z)$ . Moreover, the gauge field roaming  $\Delta\phi(z)$  is proportional to  $\frac{1}{\tilde{\kappa}^{\frac{1}{2}}\phi_0^2}$ , as also confirmed by our full numerical study (see Fig. 1).

## 4 Late time accelerated expansion, numerical analysis

Up to now, we show that the gauge-quintessence model can describe the late-time accelerated expansion of the Universe. The background trajectory is completely specified by one initial value  $\phi_0$  (as well as the sign of  $\phi'(\tilde{t}_0)$ ) and two parameters  $\tilde{g}$  and  $\tilde{\kappa}$ . Here, considering the observational best values  $\Omega_m^0 = 0.308 \pm 0.012$  and  $\Omega_r^0 \sim 10^{-4}$  [8], we explore the parameter space of our model more thoroughly. In the following, we present the result of numerical study of the field equations (3.5) for different values of  $(\phi_0, \tilde{g}, \tilde{\kappa})$ . In this section, we only consider systems with positive  $\phi'(\tilde{t}_0)$  (corresponding to  $\phi_z(z=0) < 0$ ). However, regardless of the sign of  $\phi'(\tilde{t}_0)$ , the gauge-quiescentness model can generate the late time accelerated expansion of the Universe. In the next section, we consider both cases and constrain them with the available observational data.

In the two panels shown in Fig. (1), we present the time evolution of the gauge field  $\phi$  vs. redshift. The left panel presents  $\psi(z) = \frac{\phi(z)}{\phi_0}$  ( $\phi_0 = \phi(z=0)$ ) for three different values of  $\tilde{\kappa}$ , with  $\phi_0 = 0.5$  and  $\tilde{g} = 0.01$ . In the right panel, we plot  $\psi(z)$  for three different values of the present time field,  $\phi_0$ , while we fixed the values of the parameters  $\tilde{\kappa} = 500$  and  $\tilde{g} = 0.01$ .



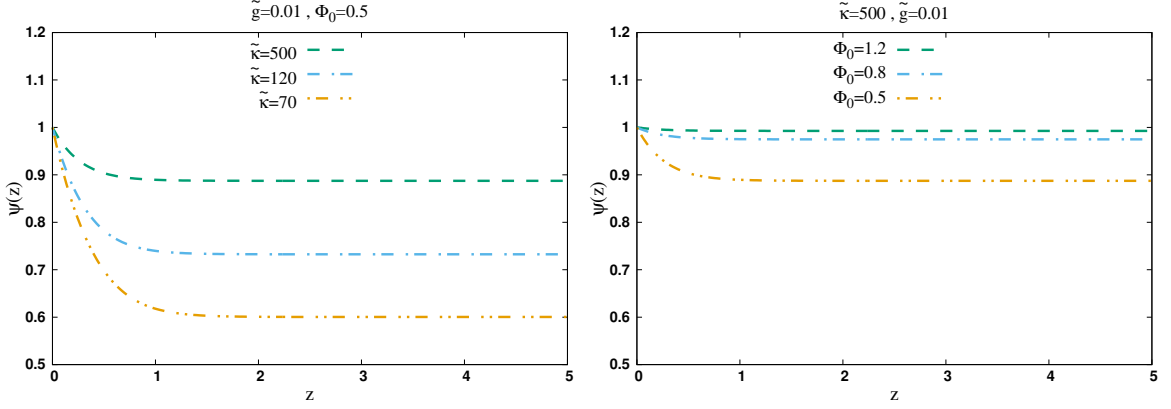


**Figure 1.** The gauge field  $\phi(z)$  evolution with respect to redshift,  $z$ . Here, we normalized each  $\phi(z)$  to its own present time value  $\phi_0$ ,  $\psi(z) = \frac{\phi(z)}{\phi_0}$ . In the left panel, we set  $(\phi_0 = 0.5, \tilde{g} = 0.01)$ , while each plot corresponds to a different value of  $\tilde{\kappa}$ . In the right panel, on the other hand, we fixed the value of parameters as  $(\tilde{\kappa} = 500, \tilde{g} = 0.01)$  for systems with three different values of  $\phi_0$ .

These plots confirm our analytical qualitative analysis in the previous section. As we see,  $\phi(z)$  is almost constant at high redshifts and during the matter dominated epoch. However, as we approach smaller redshifts, the  $\phi'(z)$  increases and thus  $\phi(z)$  evaluates faster with the redshift. As we expected from our analytical analysis, the field roaming during its evolution is related to the value of  $\tilde{\kappa}$  and  $\phi_0$  and it is proportional to  $(\tilde{\kappa}^{\frac{1}{2}}\phi_0^2)^{-1}$ .

We present the evolution of normalized density parameters, (note that in this part we normalize the density parameter by  $H^2$  rather than  $H_0^2$  see equation (3.3)), and EoS of the gauge field,  $w$ , in the right and left panels of figure (2) respectively. The *top panels* present systems with different values of  $\tilde{g}$ , while the other parameters are fixed ( $\tilde{\kappa} = 500, \phi_0 = 0.5$ ). Although the late time behaviors are roughly the same, the value of  $\tilde{g}$  affects the time evolution at higher redshifts ( $z \gg 1$ ). In particular, as we see in the upper-left panel, decreasing  $\tilde{g}$  decreases  $\Omega_G(z)$  at higher  $z$ s which is in form of (dark) radiation  $\Omega_G \propto a^{-4}$ . Note that in all these trajectories, the dark radiation density parameter is well below  $\Omega_r(z)$ . The upper-right panel zoomed in on the evolution of EoS in near redshifts. As we see, the gauge field sector is effectively a dark radiation component with EoS  $w = \frac{1}{3}$  at higher redshifts. Then, after a short transition, it takes the form of a dark energy component with EoS  $w \simeq -1$ . As we see here, the dark energy phase of the gauge field increases by decreasing  $\tilde{g}$ .

In the *middle panels*, we fix  $\phi_0 = 0.5$  and  $\tilde{g} = 0.01$  and investigate how the background trajectories are modified by changing the value of  $\tilde{\kappa}$ . The left-middle panel shows that the early  $\Omega_G(z)$  (at  $z \gg 1$ ) evaluate like radiation,  $\Omega(z) \propto a^{-4}$ , and increases by increasing  $\tilde{\kappa}$ . In the middle-right panel we then zoom in on the evolution of EoS in near redshifts. Again, at near redshifts, the gauge field sector is of the form of a dark energy component with EoS  $w \simeq -1$ , while at higher redshifts it is effectively a dark radiation component with  $w = \frac{1}{3}$ . As we see in the right panel, the dark energy phase of the gauge field increases by decreasing  $\tilde{\kappa}$ .

Finally, in the *bottom panels* of Fig.(2), we see systems with different values of  $\phi_0$ , while the other parameters are fixed ( $\tilde{\kappa} = 500, \tilde{g}^2 = 0.01$ ). This plot indicates that increasing  $\phi_0$  increases the early time  $\Omega_G(z)$  while decreases the time of the dark energy phase of the gauge field sector. The bottom-left panel shows that systems with large field values ( $\phi_0 \gtrsim 1$ ) make sizeable contribution to the total radiation during the matter era which is not consistent with



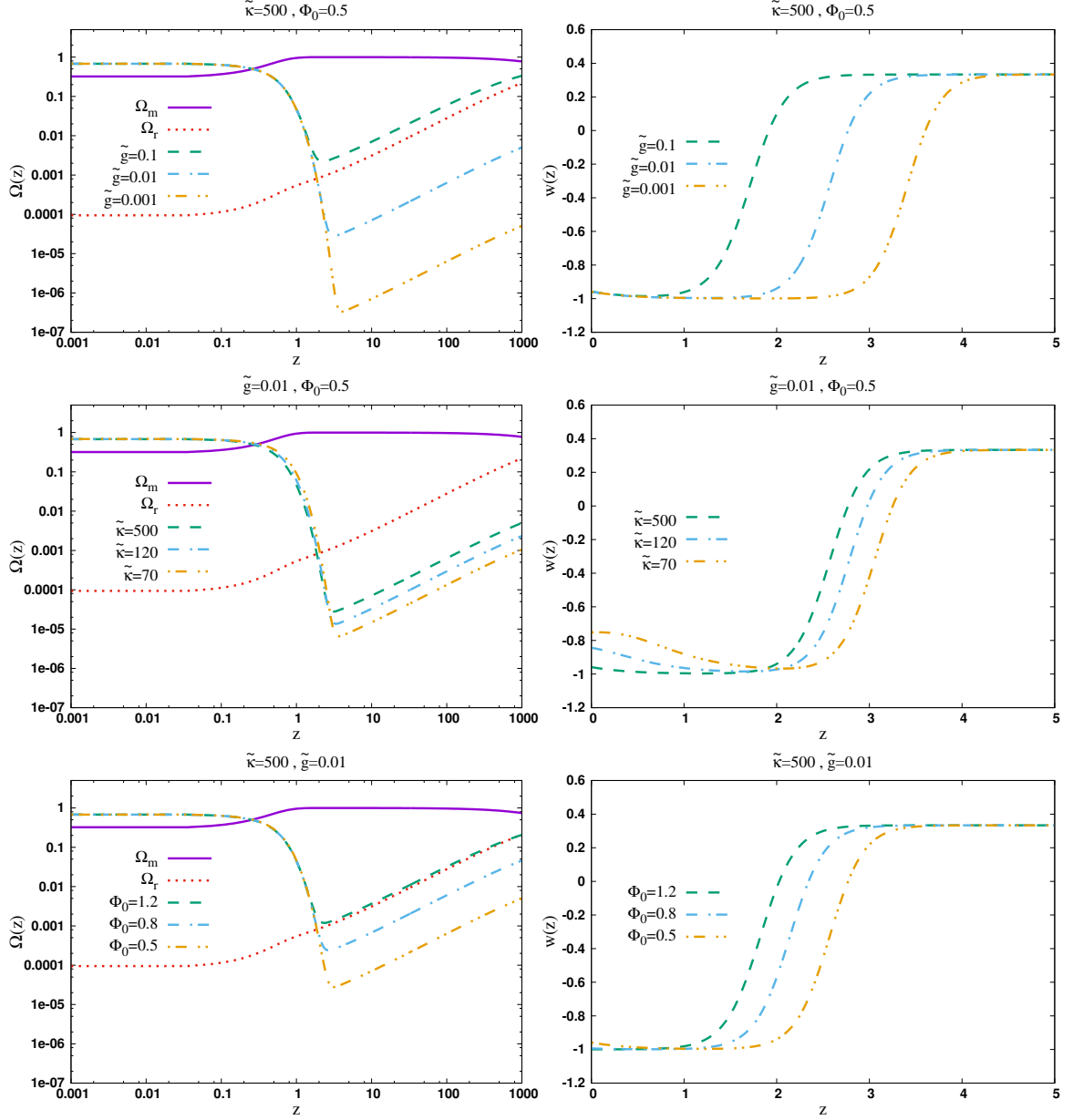


**Figure 2.** Here we explore the parameter space of the gauge-quintessence model. The left-handed panels show the density parameters for radiation  $\Omega_r$  (dotted-red line), mater  $\Omega_m$  (solid-violet line) and  $\Omega_G$  with respect to redshift  $z$ . On the right-handed panels we plotted the equation of state of the gauge sector  $w(z)$  vs.  $z$ .

observational results  $\frac{\Omega_{DR}(z)}{\Omega_r^0(z)} < 0.1$  at high redshifts. (note that with  $(\tilde{\kappa} = 500, \tilde{g}^2 = 0.01)$  but other area of parameter space may act different).

#### 4.1 Generic features of the gauge-quintessence trajectories

Our numerical analysis shows that our model can generate the late-time accelerated expansion in a large region of the parameter space. Here we summarize the generic features of these

solutions in the gauge-quintessence model where  $\Omega_m^0 = 0.308 \pm 0.012$ ,  $\Omega_G^0 = 0.69$  and the critical density  $\rho_c \equiv 3H_0^2 \sim (10^{-3}\text{ev})^4$ .

- Dynamics of the gauge-quintessence trajectories is almost insensitive to its initial field value in early times. In particular, the gauge field component acts like (dark) radiation with EoS of  $w = \frac{1}{3}$  at higher redshifts. After a sharp and fast phase transition around  $1 < z < 5$ , it however, takes the form of a dark energy component at late times.
- There is a range of parameters that the gauge field sector has an energy density a few orders of magnitude smaller than radiation. Due to the cosmic expansion, its energy density then diluted like  $a^{-4}$  at high redshifts. Thus, the gauge field sector tracks the total radiation energy density during the matter era. As we approach lower redshifts,  $\Omega_G$  increases and after a quick period of enhancement, it eventually gets constant at the dark energy era. The tracking behavior of the model attracts solutions with different initial values to a common trajectory. That makes the current energy density almost independent of the initial conditions.
- The gauge field effective value  $\phi(z)$  is almost frozen in the matter dominated era and  $\phi_z$  is negligible. However, as we approach smaller redshifts and around  $z \lesssim 5$ , the value of  $\phi'(z)$  increases and thus  $\phi(z)$  evaluates faster with the redshift. The field roaming,  $\Delta\phi(z)$ , during its evolution is related to the value of  $\tilde{\kappa}$  and  $\phi_0$  and it is proportional to  $(\tilde{\kappa}^{\frac{1}{2}}\phi_0^2)^{-1}$ .
- The energy density parameter of the gauge field sector at early times is approximately given as  $\Omega_G \simeq \frac{\tilde{g}^2\phi_0^4}{a^4}$ . Thus, the early  $\Omega_G(z)$  has a negligible  $\tilde{\kappa}$  dependent.

## 5 Contact with observational constraints

We now turn to constrain the gauge-quintessence parameters by the observational data. In this section, we study the implications of the supernovae and baryon acoustic oscillation (BAO) data sets as well as the current observational upper bounds on the early time dark sectors in our model. Finally, we compare the Taylor expansion of  $w$  with observational constraints to further constrain the model.

### 5.1 Supernovae and BAO

The observation of distant type-Ia supernovae (SnIa) is one of the most important probes of cosmic expansion. SnIa are one of our standard candles to measure luminosity distance in terms of redshift and shed great light on the late time evolution of the Universe. In this part, using SnIa and BAO data, we find the best value of free parameters of the model  $\mathbf{P} = \{\tilde{\kappa}, \tilde{g}^2, \phi_0^2\}$ . Here we used the SnIa distance module data from Union 2.1 sample [45] which includes 580 data. The  $\chi^2$  is given as

$$\chi_{\text{sn}}^2 = \sum_i \frac{[\mu_{\text{th}}(z_i) - \mu_{\text{ob}}(z_i)]^2}{\sigma_i^2}, \quad (5.1)$$

where

$$\mu(z) = 5 \log_{10} \left[ (1+z) \int_0^z \frac{dx}{E(x)} \right] + \mu_0,$$

$z$	$d(z)$	Survey
0.106	0.336	6dFGS [48]
0.35	0.113	SDSS-DR7 [49]
0.57	0.073	SDSS-DR9 [50]
0.44	0.0916	WiggleZ [51]
0.6	0.0726	WiggleZ [51]
0.73	0.0592	WiggleZ [51]

**Table 1.** The BAO data which are used in this analyze.

is distance module,  $\sigma_i$  is its uncertainty and  $\mu_0 = 42.384 - 5 \log_{10} h$ . It is useful to expand the SnIa  $\chi^2$  around  $\mu_0$  as

$$\chi_{\text{sn}}^2 = A + 2B\mu_0 + C\mu_0^2, \quad (5.2)$$

where

$$A = \sum_i \frac{[\mu_{\text{th}}(z_i) - \mu_{\text{ob}}(z_i)]^2}{\sigma_i^2} \Big|_{\mu_0=0}, \quad B = \sum_i \frac{[\mu_{\text{th}}(z_i) - \mu_{\text{ob}}(z_i)]}{\sigma_i^2} \Big|_{\mu_0=0} \quad \text{and} \quad C = \sum_i \frac{1}{\sigma_i^2}.$$

We use the minimum of (5.2),  $\tilde{\chi}_{\text{sn}}^2 = A - \frac{B^2}{C}$ , to obtain the best values of our parameters. Note that  $\tilde{\chi}_{\text{sn}}^2$  is independent of  $\mu_0$  and it has been shown in [46] that both approaches give the same results.

Baryon acoustic oscillations (BAO) are the frozen leftovers of the oscillations in the relic baryon-photon plasma on the matter power spectrum [47]. Since the scale of BAO is very large (with the comoving scale  $l_{\text{BAO}} \simeq 100h^{-1}\text{Mpc}$ ), up to a very good approximation, it is governed by linear, well-understood physics. That made BAO the next-most robust cosmological probe after CMB fluctuations. In fact, BAO is a powerful standard measure which can provide both angular distance,  $D_A(z)$ , and Hubble parameter,  $H(z)$ , using almost linear physics and offers constraints on the background evolution of dark energy.

Here, it is useful to introduce the following distance ratio

$$d(z) = \frac{r_s(z_d)}{D_V(z)}, \quad (5.3)$$

in which  $z_d$  is the redshift of drag epoch,  $D_V(z)$  is a geometric estimate of the effective distance, defined as

$$D_V(z) = \left( (1+z)^2 D_A^2(z) \frac{z}{H(z)} \right)^{\frac{1}{3}}, \quad (5.4)$$

and  $r_s(a)$  is the comoving sound horizon

$$r_s(a) = \int_0^a \frac{c_s da}{a^2 H(a)} \quad \text{where} \quad c_s(a) = \frac{1}{\sqrt{3(1 + \frac{3\Omega_b^0}{4\Omega_\gamma^0} a)}}, \quad (5.5)$$

where  $c_s$  is the baryon sound speed. We set the  $z_d$  fitting formula from [52]. BAO has been measured in some different redshifts. In Tab. (1), we presented the current available data. Following [53], we can incorporate the BAO data into  $\chi^2$  below

$$\chi_{\text{BAO}}^2 = \mathbf{Y}^T \mathbf{C}_{\text{BAO}}^{-1} \mathbf{Y}, \quad (5.6)$$

Parameters	$\chi^2_{min}/nof$	$\tilde{\kappa}$	$\tilde{g}^2$	$\phi_0^2$
Model A	$\frac{567.2}{580}$	$1055.4^{+\infty}_{-800.2}$	$0.000016^{+0.000045}_{-0.000016}$	$0.36^{+2.15}_{-0.28}$
Model B	$\frac{567.6}{580}$	$1255.7^{+\infty}_{-1253.2}$	$0.000012^{+0.000065}_{-0.000012}$	$2.35^{+7.55}_{-2.29}$

**Table 2.**  $1\sigma$  limits on our free parameters  $\{\tilde{\kappa}, \tilde{g}^2, \phi_0^2\}$  and  $\chi^2_{min}$  using the SnIa distance module data from Union 2.1 sample [45] and BAO data. Model A and B correspond to systems with positive and negative  $\phi'(t_0)$  respectively.

where  $\mathbf{Y}$  is given as

$$\mathbf{Y} = (d(0.1) - d_1, \frac{1}{d(0.35)} - \frac{1}{d_2}, \frac{1}{d(0.57)} - \frac{1}{d_3}, d(0.44) - d_4, d(0.6) - d_5, d(0.73) - d_6). \quad (5.7)$$

Moreover from [53], the covariance matrix  $\mathbf{C}_{BAO}^{-1}$  in Eq. (5.6) is

$$\mathbf{C}_{BAO}^{-1} = \begin{pmatrix} 4444.4 & 0. & 0. & 0. & 0. & 0. \\ 0. & 34.602 & 0. & 0. & 0. & 0. \\ 0. & 0. & 20.6611 & 0. & 0. & 0. \\ 0. & 0. & 0. & 24532.1 & -25137.7 & 12099.1 \\ 0. & 0. & 0. & -25137.7 & 134598.4 & -64783.9 \\ 0. & 0. & 0. & 12099.1 & -64783.9 & 128837.6 \end{pmatrix}.$$

Recalling that the overall likelihood function of two individual likelihoods is given by their products,  $\mathcal{L}_{tot} = \mathcal{L}_{sn} \times \mathcal{L}_{BAO}$ , we obtain the total  $\chi^2$  as

$$\chi^2_{tot} = \tilde{\chi}^2_{sn} + \chi^2_{BAO}. \quad (5.8)$$

We then perform a MCMC (Monte Carlo Markov Chains) analysis of the available SnIa and BAO to find the minimum of  $\chi^2_{tot}$  as well as the best values of parameters and their uncertainties. The results are summarized in Table (2) where model A (B) corresponds to systems with positive (negative) values of  $\phi'(t_0)$ . We present the  $1\sigma$  and  $2\sigma$  confidence regions and likelihood functions in Fig. (3). As we see, the data leads to an upper bound on the value of  $\tilde{\kappa}$ , a lower bound on  $\tilde{g}^2$  and an interval for  $\phi_0^2$ . In particular, the  $1\sigma$  confidence level constrains model A parameters as  $\tilde{\kappa} \gtrsim 50$ ,  $\tilde{g}^2 \lesssim 6 \times 10^{-5}$  and  $0.1 < \phi_0^2 < 2$ . Moreover, for model B, we have  $\tilde{\kappa} \gtrsim 2$ ,  $\tilde{g}^2 \lesssim 7.7 \times 10^{-5}$  and  $0.1 < \phi_0^2 < 10$ . It is noteworthy to mention that although both models are the same in fitting with the data, model B has a relatively bigger confidence regions comparing to model A.

## 5.2 Dark energy density at early times

One of the main goals in understanding dark energy is to measure  $\Omega_{DE}(z)$  in different redshifts. Up to now, we mainly focus on the late time effects of DE. However, the early time dark energy (EDE), the amount of DE presented in the early times  $\Omega_e$ , can influence CMB anisotropies, structure formation and CMB lensing. In particular, EDE reduces the growth of structures after last scattering and generates less clusters comparing to  $\Lambda$ CDM. That then leads to a weaker lensing potential to influence the high  $l$  anisotropies. The current upper bound on the abundance of DE density in the last scattering surface is  $\Omega_e(z_{lss}) \lesssim 0.01$  (95% CL) [8]. It is noteworthy to mention that for  $\Lambda$ CDM, the early contribution of dark energy is  $\Omega_\Lambda(z_{lss}) \approx 10^{-9}$ .

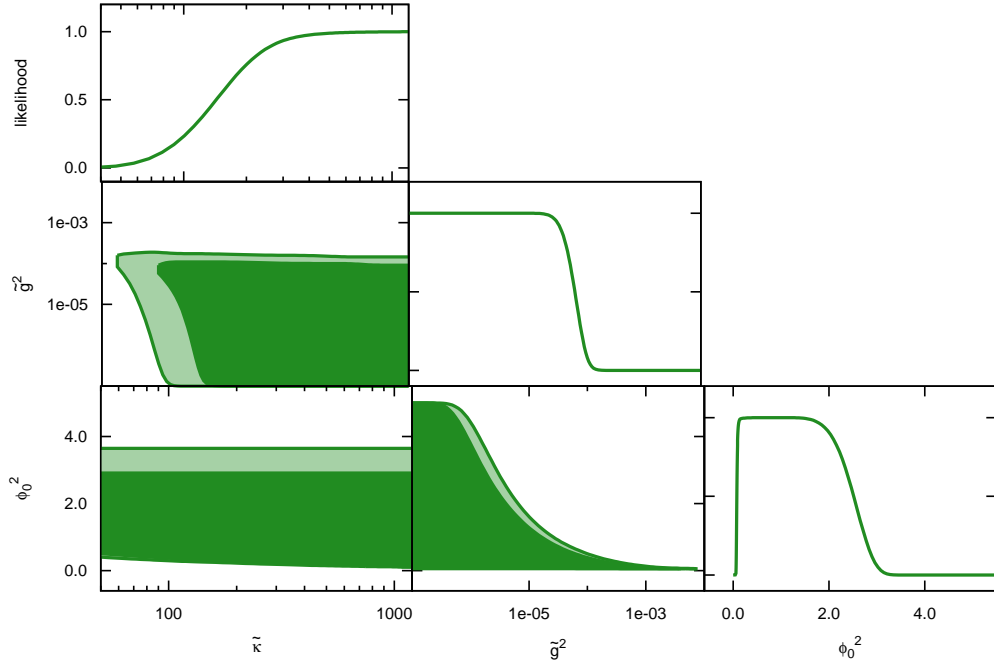


**Figure 3.**  $1\sigma$  and  $2\sigma$  contour plot for the model parameters. The likelihood functions for each parameters are shown by solid line.

Any forms of early relativistic dark sectors, dark radiation (DR), is observable through its contribution to the radiation density in the universe. The energy contribution of the early relativistic degrees of freedom is parametrized by the effective number of light species  $N_{\text{eff}}$ , as

$$N_{\text{eff}} \equiv \frac{8}{7} \left( \frac{11}{4} \right)^{\frac{4}{3}} \frac{\rho_{\text{light}}}{\rho_r} \quad (5.9)$$

where  $\rho_r$  is the energy density of photons, while  $\rho_{\text{light}}$  is the total relativistic energy density in neutrinos and DR at  $T \ll 1$  MeV respectively. Since neutrinos are slightly heated and not fully decoupled at the electron-positron annihilation, the cosmological prediction for effective number of neutrinos is  $N_\nu = 3.046$  [54]. Thus, in case that all the relativistic degrees of freedom are SM neutrinos, the numerical factor is  $N_{\text{eff}} = 3.046$ . However, observational data constraints the effective relativistic degrees of freedom as  $N_{\text{eff}} = 3.15 \pm 0.23$  [8]. Although that number is consistent with the standard value of 3.046, a significant density of extra radiation is still allowed which may indicate new physics,  $\Delta N_{\text{eff}} = 0.1 \pm 0.23$ . On the other hand, from (5.9) and after using the SM neutrinos  $N_\nu$ , we have the following relation for the effective (dark) radiation degrees of freedom  $\Delta N_{\text{eff}}$

$$\Delta N_{\text{eff}} \simeq \frac{3}{2} \frac{\Omega_{\text{DR}}}{\Omega_r}. \quad (5.10)$$

In other words, the Yang-Mills sector of the dark gauge field contributes to the effective relativistic degrees of freedom. Using the current observational constraint ( $\Delta N_{\text{eff}} = 0.1 \pm$

0.23), we obtain an upper bound on the ratio of DR density to radiation density at early times,  $\frac{\Omega_{\text{DR}}}{\Omega_r} \lesssim 0.2$ .

Coming back to our model, as we showed in the previous section, the gauge field sector acts like a dark energy term with  $w \simeq -1$  at late times  $z \lesssim 5$ . However, at the early times  $z \gtrsim 5$ , it behaves like a (dark) radiation component with EoS equal to  $w = \frac{1}{3}$ . Thus, in the gauge-quintessence trajectories, the early DE density  $\Omega_e = 0$ , while the gauge field generates an early radiation density  $\Omega_G = \Omega_{DR}$  at high redshifts. As indicated by our numerical analysis, the gauge field  $\phi$  is almost constant at redshifts higher than 10 ( $\phi'(z) \simeq 0$  where  $z \gg 1$ ), while the total field roaming  $\frac{\Delta\phi}{\phi_0}$  (from early times until present) is about 20%. That then leads to the following approximations for the early time energy density parameters

$$\Omega_G(z) \simeq \Omega_{\text{DR}}(z) \sim \frac{1}{2} \frac{\tilde{g}^2 \phi_0^4}{a^4} \quad \text{and} \quad \Omega_r(z) = \frac{\Omega_r^0}{a^4}. \quad (5.11)$$

Using the observational upper bound on the value of  $\Delta N_{\text{eff}}$  and  $\Omega_r^0$ , we then obtain

$$\tilde{g}^2 \phi_0^4 \simeq \frac{4}{3} \Omega_r^0 \Delta N_{\text{eff}} \lesssim 10^{-5}. \quad (5.12)$$

In the following, we use the above upper bound to further constrain the parameter space.

### 5.3 Taylor expansion of $w$

One of the key points in understanding the nature of the late-time accelerated expansion is the value of  $w$ . This quantity is equal to  $-1$  for the cosmological constant and any deviation from that implies new physics. As a quintessence model, gauge-quintessence has a redshift dependent equation of state. As we showed in the previous section,  $w$  is  $\frac{1}{3}$  at high redshifts and then after a short phase transition, EoS gets close to  $-1$ . After  $z = 1$ , the EoS is very slow varying and  $w(z)$  is well described by its 1st order Taylor expansion around  $z = 0$ . In order to test the time-varying EoS, we expand  $w(z)$  in a Taylor series, as discussed in [8]

$$w(z) \simeq w_0 + w_a \frac{z}{1+z}. \quad (5.13)$$

Expanding  $w(z)$  in (2.4) and after using the fact that  $\tilde{g}^2 \phi_0^4 \ll \phi_0'^2$ , we obtain  $\delta w_0$  and  $w_a$  as

$$w_0 = -1 + \delta w_0 \quad \text{where} \quad \delta w_0 = \frac{4}{3} \frac{1}{\kappa \phi_0^4}, \quad (5.14a)$$

$$w_a^{A,B} = \frac{16}{3} \frac{(\frac{\phi_0'}{\phi_0} - 1) \kappa \phi_0^4}{(1 + \kappa \phi_0^4)^2} \simeq 4 \left( \frac{\sigma_{A,B} \delta w_0^{\frac{1}{2}}}{\phi_0} - 1 \right) \delta w_0, \quad \text{where} \quad \sigma_{A,B} = \pm 1, \quad (5.14b)$$

where in the last equality in the 2nd line, we used (3.7) and the fact that  $\kappa \phi_0^4 \gg 1$ . Note that in our model,  $w_0 > -1$  and hence  $\delta w_0$  is always positive.

The  $1\sigma$  constraints of *Planck*+BAO+SN-Ia+ $H_0$  (68% CL) [8] gives the current constraints as  $-0.1 < \delta w_0 < 0.2$  and  $-1 < w_a < 0.2$ . Considering the best value of parameters in model A and B we found ( $\delta w_0 = 2.5 \times 10^{-3}$ ,  $w_a = 8.7 \times 10^{-3}$ ) and ( $\delta w_0 = 1. \times 10^{-4}$ ,  $w_a = 4 \times 10^{-4}$ ) respectively, which are very close to  $\Lambda$ CDM model.

## 6 A quick treatment of the perturbations

Up to now, we have studied the background evolution of the gauge-quintessence model, including  $w(z)$  and  $\Omega_{DE}(z)$ . Although, our model is close to  $\Lambda$ CDM at the background level, perturbations may still evolve differently and provides a fingerprint for the model. In particular, the (dark) gauge field sector contributes to the cosmic perturbations and may affect the galaxy clustering and weak lensing. In this sector, we investigate the qualitative behavior of the linear cosmic perturbation of our model which capture the main features of the models. The precise full numeric study of the fluctuations is beyond the scope of the present paper and we postpone it for future work.

As the large-scale structure and weak lensing surveys are measuring the matter-density contrast and the gravitational potentials, we therefore focus on scalar perturbations here. Using the Newtonian gauge, the scalar sector of the perturbed FRW metric can be parametrized as

$$ds^2 = -(1 + 2\Phi)dt^2 + a^2(1 - 2\Psi)\delta_{ij}dx^i dx^j. \quad (6.1)$$

Thus, the space-time metric is fully specified by three quantities  $\{H(t), \Psi(t, \vec{x}), \Phi(t, \vec{x})\}$ : two Bardeen potentials,  $\Psi$  and  $\Phi$ , as well as the Hubble parameter, given as (neglecting radiation)

$$H^2(z) = H_0^2 \left( \Omega_m^0 (1+z)^3 + (1 - \Omega_m^0) \exp \left( 3 \int_0^z (1+w(z')) d \ln(1+z) \right) \right), \quad (6.2)$$

where  $w$  is the EoS of dark sector. Note that  $\Phi$  is the Newtonian potential and in the absence of anisotropic stress in general relativity, e.g.  $\Lambda$ CDM, we have  $\Psi = \Phi$ . However, in most of modified gravity models and some dark energy models including vector and gauge fields, we may have a non zero anisotropic stress.

### 6.1 Anisotropic stress

The gravitational lensing is sensitive to the combination of  $\Phi + \Psi$ , while the anisotropic clustering of galaxies in redshift space measures the peculiar velocity which is related to  $\Psi$ . Thus, the combination of them makes us able to determine both  $\Psi$  and  $\Phi$ . From the theory on the other hand, the off-diagonal spatial part of the linear perturbed Einstein equation gives

$$\Psi = \Phi + \Pi^s, \quad (6.3)$$

where  $\Pi^s$  is the scalar anisotropic stress, given as  $\delta T_j^i - \frac{1}{3}\delta_j^i \delta T_j^j = (\partial_{ij} - \frac{1}{3}\nabla^2)\Pi^s$ . As a result, presence of anisotropic stress leads to inequality of the Bardeen potentials. In particular, the relativistic particles, i.e. photons, neutrinos and dark radiation contributes to  $\Pi^s$ , generating a non-zero scalar anisotropic stress. The background cosmic neutrino fluctuations and any possible freestreaming particles generate significant anisotropic stress which induces a characteristic phase shift in the acoustic peaks of CMB [41]. This phase shift recently has been detected in [55] and future CMB observations will improve our understanding about them. In our model, on the other hand, due to its self interactions, the dark sector is well described as a perfect fluid with  $c_{\text{vis}}^2 = 0$  rather than a free-streaming component with  $c_{\text{vis}}^2 = \frac{1}{3}$ . As a result, the gauge field sector has a negligible contribution to the anisotropic stress,  $\Psi = \Phi$ .

### 6.2 Cosmic structure formation and the dark sector

Cosmic structure formation is another way to explore the dark energy models besides the expansion history. Linear perturbations governed by the well-known physics and free of



many astrophysical complexities. We can write the small fluctuations to the homogeneous energy density ( $\bar{\rho}_m(t)$ ) and the Hubble flow velocity  $Hx^i$  as below

$$\rho_m(t, \vec{x}) = (1 + \delta_m(t, \vec{x}))\bar{\rho}_m(t), \quad \text{and} \quad v^i = Hx^i + \partial_i u(t, \vec{x}), \quad (6.4)$$

where overbars denotes background quantities,  $\delta_m$  is the fractional density contrast of the dark matter and  $\vec{u}$  is its peculiar velocity. The linear order continuity and Euler equations govern the evolution of  $\delta_m$  and  $u_m$  which are respectively as below

$$\dot{\delta}_m + \frac{1}{a}\partial^2 u_m = 0 \quad \text{and} \quad \dot{u}_m + H u_m + \frac{1}{a}\Psi = 0. \quad (6.5)$$

Moreover, the Poisson equation gives  $\Psi$  in terms of the total energy density as

$$k^2 \Psi = -4\pi G a^2 \bar{\rho}_m \left( \delta_m + \frac{\bar{\rho}_G}{\bar{\rho}_m} \delta_G \right), \quad (6.6)$$

where  $\delta_G$  is the density contrast of the dark gauge field [23]. Standard inflation models predicts that the initial conditions are adiabatic, which in the absence of isocurvature fluctuations implies that our fluctuations are adiabatic and we have  $\delta_G = (1 + w_G)\delta_m$ . From the combination of (6.5) and (6.6), we then obtain a dynamical field equation for  $\delta_m$

$$\ddot{\delta}_m + 2H\dot{\delta}_m = 4\pi G \bar{\rho}_m Q(t) \delta_m \quad \text{where} \quad Q(t) = \left( 1 + \frac{\bar{\rho}_G(t)}{\bar{\rho}_m(t)} (1 + w_G(t)) \right). \quad (6.7)$$

Note that  $Q - 1$  is the deviation of dark matter evolution from  $\Lambda$ CDM prediction.

In our model, around  $z \lesssim 5$  the gauge field sector effectively acts like a dark energy sector with  $w_G \simeq -1$ . Moreover, the ratio  $\frac{\bar{\rho}_G}{\bar{\rho}_m}$  is negligible for  $z \gtrsim 1$  which implies that  $Q(z) - 1$  is almost zero at that regime and the Hubble parameter (6.2) is equal to the  $\Lambda$ CDM one,  $H_\Lambda(z)$ . Thus, during the matter era, the structure formation is almost exactly the same as  $\Lambda$ CDM,  $\delta_m = \delta_0 a$  in our model. On the other hand, around  $z = 0.5$ , dark energy dominates over matter and the energy density ratio becomes equal to  $\frac{1 - \Omega_m^0}{\Omega_m^0(1+z)^3}$ . Upon using (5.14) in (6.7), we then obtain  $Q(z)$  and  $H(z)$  as below for  $z \lesssim 1$

$$Q(z) = 1 + \frac{1 - \Omega_m^0}{\Omega_m^0(1+z)^3} \delta w_0 \geq 0 \quad (\delta w_0 \geq 0), \quad (6.8a)$$

$$H(z) = H_\Lambda(z) \left( 1 + \frac{3}{2} \frac{(1 - \Omega_m^0) \delta w_0 z}{((1 - \Omega_m^0) + \Omega_m^0(1+z)^3)} \right). \quad (6.8b)$$

Note that in order to write  $H(z)$  (equation (6.2)) in terms of its corresponding  $\Lambda$ CDM Hubble parameter  $H_\Lambda(z)$ , we used the fact that the  $w(z)$  expansion (5.13) is valid at  $z < 1$ . Similar to the standard quintessence models, our model has a sound speed very close to one, and does not cluster significantly inside the horizon. Equation (6.8) implies that the time varying EoS increases both of the source term  $Q\rho_m$  and the Hubble friction comparing with the  $\Lambda$ CDM. However, recalling that  $0 < \delta w_0 \sim 10^{-3}$  for our best fits, this effect is not significant.

## 7 Discussion and Conclusions

In this paper, we investigated the cosmological evolution of a novel quintessence scenario, *gauge-quintessence*. Our dark energy candidate is a self-interacting (dark) gauge field which

interacts gravitationally with the visible Universe and minimally coupled to Einstein gravity. The gauge field theory of the model consists of the standard Yang-Mills with an EoS equal to  $\frac{1}{3}$ , and  $\kappa(F\tilde{F})^2$  term which effectively is a dark energy sector. The (dark) gauge sector has two free parameters, the gauge field coupling  $g$  and the dimensionful  $\kappa$  which has the dimension of  $\text{mass}^{-4}$ . Thus, in the regime that the  $\kappa$ -term dominates, the dark gauge sector acts like a quintessence model, justifying the name gauge-quintessence. Our gauge field theory, originally, has been introduced and studied as an inflationary model to describe the early time exponential expansion after the big bang in [29, 30], as gauge-flation. Here, we examined the late time cosmology of the model in the presence of matter and radiation to explain the late time accelerated expansion of the Universe.

We performed a likelihood analysis to compare the available SnIa and BAO data with the gauge-quintessence model and find the best values of our parameters. Our model can describe the late-time dark energy era over a wide range of its parameter space. During the radiation and early matter eras, the gauge field sector acts like (dark) radiation and dilutes like  $a^{-4}$ . We then have a quick transition period in which  $w$  sharply decreases from  $\frac{1}{3}$  to  $-1$ , while its energy density parameter increases rapidly. Eventually, at low-redshifts, the gauge field sector takes the form of a dark energy and its energy density becomes the dominant part of the energy budget of the Universe,  $\Omega_G \simeq 0.7$ . Due to the tracking feature of our model, solutions with different initial values are attracted to a common trajectory. That makes the current energy density almost independent of the initial conditions. The effective field value  $\phi(z)$  is almost frozen during the radiation and matter eras, while as we approach smaller redshifts ( $z \lesssim 5$ ), it starts to evaluate faster with time. The total field roaming of the gauge field,  $\Delta\phi(z)$ , is about or less than 10% for the acceptable systems.

The presence of early dark radiation (EDR) is a robust prediction of our model. Our gauge quintessence model act like a radiation component at early time and may have a contribution to the total radiation energy density. During the recombination era, the energy density of EDR manifests itself observationally as a contribution to the effective number of neutrino species,  $N_{\text{eff}}$ . The current constraint on the effective relativistic degrees of freedom from the Planck satellite is  $N_{\text{eff}} = 3.15 \pm 0.23$  [7], while the SM prediction is  $N_{\text{eff}}^{\text{SM}} = 3.046$ . That then leads to  $\Delta N_{\text{eff}} = 0.1 \pm 0.23$  which may indicates new relativistic degrees of freedom at the time of recombination. Future CMB polarization experiments will improve our constraints on  $\Delta N_{\text{eff}}$  by one or two order of magnitude [44]. Using the current observational constraint on  $\Delta N_{\text{eff}}$  to our model, we obtain  $g^2\phi_0^4 \lesssim 10^{-5}H_0^2$ .

## Acknowledgments

We greatly appreciate M. M. Sheikh-Jabbari for his valuable comments on the manuscript. Work of A. MN. is supported in part by the grant from *Boniad Melli Nokhbegan of Iran*. A. MN. acknowledges the hospitality of the Aspen Center for Physics and support from PHY-1066293.

## References

- [1] **Supernova Search Team** Collaboration, A. G. Riess et al., *Observational evidence from supernovae for an accelerating universe and a cosmological constant*, *Astron. J.* **116** (1998) 1009–1038, [[astro-ph/9805201](#)].

- [2] **Supernova Cosmology Project** Collaboration, S. Perlmutter et al., *Measurements of Omega and Lambda from 42 high redshift supernovae*, *Astrophys.J.* **517** (1999) 565–586, [[astro-ph/9812133](#)].
- [3] A. G. Riess et al., *BV RI light curves for 22 type Ia supernovae*, *Astron. J.* **117** (1999) 707–724, [[astro-ph/9810291](#)].
- [4] **SDSS Collaboration** Collaboration, M. Tegmark et al., *Cosmological parameters from SDSS and WMAP*, *Phys.Rev.* **D69** (2004) 103501, [[astro-ph/0310723](#)].
- [5] **SDSS Collaboration** Collaboration, M. Tegmark et al., *Cosmological Constraints from the SDSS Luminous Red Galaxies*, *Phys.Rev.* **D74** (2006) 123507, [[astro-ph/0608632](#)].
- [6] **WMAP Collaboration** Collaboration, D. Spergel et al., *First year Wilkinson Microwave Anisotropy Probe (WMAP) observations: Determination of cosmological parameters*, *Astrophys.J.Suppl.* **148** (2003) 175–194, [[astro-ph/0302209](#)].
- [7] **Planck** Collaboration, P. A. R. Ade et al., *Planck 2015 results. XIII. Cosmological parameters*, [arXiv:1502.01589](#).
- [8] **Planck Collaboration** Collaboration, P. Ade et al., *Planck 2015 results. XIV. Dark energy and modified gravity*, [arXiv:1502.01590](#).
- [9] W. J. Percival, S. Cole, D. J. Eisenstein, R. C. Nichol, J. A. Peacock, A. C. Pope, and A. S. Szalay, *Measuring the Baryon Acoustic Oscillation scale using the SDSS and 2dFGRS*, *Mon. Not. Roy. Astron. Soc.* **381** (2007) 1053–1066, [[arXiv:0705.3323](#)].
- [10] Å. Aubourg et al., *Cosmological implications of baryon acoustic oscillation (BAO) measurements*, [arXiv:1411.1074](#).
- [11] D. Huterer et al., *Growth of Cosmic Structure: Probing Dark Energy Beyond Expansion*, *Astropart. Phys.* **63** (2015) 23–41, [[arXiv:1309.5385](#)].
- [12] A. Hojjati and E. V. Linder, *CMB Lensing and Scale Dependent New Physics*, [arXiv:1507.08292](#).
- [13] S. Weinberg, *The Cosmological Constant Problem*, *Rev. Mod. Phys.* **61** (1989) 1–23.
- [14] S. Nobbenhuis, *The Cosmological Constant Problem, an Inspiration for New Physics*. PhD thesis, Utrecht U., 2006. [gr-qc/0609011](#).
- [15] V. Sahni and A. A. Starobinsky, *The Case for a positive cosmological Lambda term*, *Int.J.Mod.Phys.* **D9** (2000) 373–444, [[astro-ph/9904398](#)].
- [16] P. Peebles and B. Ratra, *The Cosmological constant and dark energy*, *Rev.Mod.Phys.* **75** (2003) 559–606, [[astro-ph/0207347](#)].
- [17] S. M. Carroll, *The Cosmological constant*, *Living Rev. Rel.* **4** (2001) 1, [[astro-ph/0004075](#)].
- [18] S. Tsujikawa, *Dark energy: investigation and modeling*, [arXiv:1004.1493](#).
- [19] E. J. Copeland, M. Sami, and S. Tsujikawa, *Dynamics of dark energy*, *Int.J.Mod.Phys.* **D15** (2006) 1753–1936, [[hep-th/0603057](#)].
- [20] A. De Felice and S. Tsujikawa, *f(R) theories*, *Living Rev. Rel.* **13** (2010) 3, [[arXiv:1002.4928](#)].
- [21] S. Tsujikawa, *Modified gravity models of dark energy*, *Lect. Notes Phys.* **800** (2010) 99–145, [[arXiv:1101.0191](#)].
- [22] T. Clifton, P. G. Ferreira, A. Padilla, and C. Skordis, *Modified Gravity and Cosmology*, *Phys. Rept.* **513** (2012) 1–189, [[arXiv:1106.2476](#)].
- [23] **Euclid Theory Working Group** Collaboration, L. Amendola et al., *Cosmology and fundamental physics with the Euclid satellite*, *Living Rev. Rel.* **16** (2013) 6, [[arXiv:1206.1225](#)].

- [24] T. Clifton, P. G. Ferreira, A. Padilla, and C. Skordis, *Modified gravity and cosmology*, *Phys. Rep.* **513** (Mar., 2012) 1–189, [[arXiv:1106.2476](#)].
- [25] Y.-S. Song, A. Taruya, E. Linder, K. Koyama, C. G. Sabiu, G.-B. Zhao, F. Bernardeau, T. Nishimichi, and T. Okumura, *Consistent Modified Gravity Analysis of Anisotropic Galaxy Clustering Using BOSS DR11*, *Phys. Rev.* **D92** (2015), no. 4 043522, [[arXiv:1507.01592](#)].
- [26] G. Gubitosi, F. Piazza, and F. Vernizzi, *The Effective Field Theory of Dark Energy*, *JCAP* **1302** (2013) 032, [[arXiv:1210.0201](#)]. [JCAP1302,032(2013)].
- [27] S. Tsujikawa, *Quintessence: A Review*, *Class. Quant. Grav.* **30** (2013) 214003, [[arXiv:1304.1961](#)].
- [28] I. Zlatev, L.-M. Wang, and P. J. Steinhardt, *Quintessence, cosmic coincidence, and the cosmological constant*, *Phys. Rev. Lett.* **82** (1999) 896–899, [[astro-ph/9807002](#)].
- [29] A. Maleknejad and M. Sheikh-Jabbari, *Gauge-flation: Inflation From Non-Abelian Gauge Fields*, *Phys.Lett.* **B723** (2013) 224–228, [[arXiv:1102.1513](#)].
- [30] A. Maleknejad and M. Sheikh-Jabbari, *Non-Abelian Gauge Field Inflation*, *Phys.Rev.* **D84** (2011) 043515, [[arXiv:1102.1932](#)].
- [31] M. Sheikh-Jabbari, *Gauge-flation Vs Chromo-Natural Inflation*, *Phys.Lett.* **B717** (2012) 6–9, [[arXiv:1203.2265](#)].
- [32] J. Bielefeld and R. R. Caldwell, *Cosmological consequences of classical flavor-space locked gauge field radiation*, *Phys. Rev.* **D91** (2015), no. 12 124004, [[arXiv:1503.05222](#)].
- [33] D. V. Gal'tsov and E. A. Davydov, *Cosmological models with gauge fields*, *Proc. Steklov Inst. Math.* **272** (2011) 119–140, [[arXiv:1012.2861](#)].
- [34] M. Rinaldi, *Dark energy as a fixed point of the Einstein Yang-Mills Higgs Equations*, [[arXiv:1508.04576](#)].
- [35] M. A. Buen-Abad, G. Marques-Tavares, and M. Schmaltz, *Non-Abelian dark matter and dark radiation*, *Phys. Rev.* **D92** (2015), no. 2 023531, [[arXiv:1505.03542](#)].
- [36] C. Gross, O. Lebedev, and Y. Mambrini, *Non-Abelian gauge fields as dark matter*, *JHEP* **08** (2015) 158, [[arXiv:1505.07480](#)].
- [37] H. Zhang, C. S. Li, Q.-H. Cao, and Z. Li, *A Dark Matter Model with Non-Abelian Gauge Symmetry*, *Phys. Rev.* **D82** (2010) 075003, [[arXiv:0910.2831](#)].
- [38] A. Maleknejad, M. Sheikh-Jabbari, and J. Soda, *Gauge Fields and Inflation*, *Phys.Rept.* **528** (2013) 161–261, [[arXiv:1212.2921](#)].
- [39] P. Adshead and M. Wyman, *Chromo-Natural Inflation: Natural inflation on a steep potential with classical non-Abelian gauge fields*, *Phys.Rev.Lett.* **108** (2012) 261302, [[arXiv:1202.2366](#)].
- [40] E. Martinec, P. Adshead, and M. Wyman, *Chern-Simons EM-flation*, *JHEP* **02** (2013) 027, [[arXiv:1206.2889](#)].
- [41] D. Baumann, D. Green, J. Meyers, and B. Wallisch, *Phases of New Physics in the CMB*, [[arXiv:1508.06342](#)].
- [42] L. Ackerman, M. R. Buckley, S. M. Carroll, and M. Kamionkowski, *Dark Matter and Dark Radiation*, *Phys. Rev.* **D79** (2009) 023519, [[arXiv:0810.5126](#)]. [,277(2008)].
- [43] J. Lesgourgues, G. Marques-Tavares, and M. Schmaltz, *Evidence for dark matter interactions in cosmological precision data?*, [[arXiv:1507.04351](#)].
- [44] W. L. K. Wu, J. Errard, C. Dvorkin, C. L. Kuo, A. T. Lee, P. McDonald, A. Slosar, and O. Zahn, *A Guide to Designing Future Ground-based Cosmic Microwave Background Experiments*, *Astrophys. J.* **788** (2014) 138, [[arXiv:1402.4108](#)].

- [45] N. Suzuki et al., *The Hubble Space Telescope Cluster Supernova Survey: V. Improving the Dark Energy Constraints Above  $z > 1$  and Building an Early-Type-Hosted Supernova Sample*, *Astrophys. J.* **746** (2012) 85, [[arXiv:1105.3470](#)].
- [46] S. Nesseris and L. Perivolaropoulos, *Comparison of the legacy and gold snia dataset constraints on dark energy models*, *Phys. Rev. D* **72** (2005) 123519, [[astro-ph/0511040](#)].
- [47] B. A. Bassett and R. Hlozek, *Baryon Acoustic Oscillations*, [arXiv:0910.5224](#).
- [48] F. Beutler, C. Blake, M. Colless, D. H. Jones, L. Staveley-Smith, et al., *The 6dF Galaxy Survey: Baryon Acoustic Oscillations and the Local Hubble Constant*, *Mon.Not.Roy.Astron.Soc.* **416** (2011) 3017–3032, [[arXiv:1106.3366](#)].
- [49] N. Padmanabhan, X. Xu, D. J. Eisenstein, R. Scalzo, A. J. Cuesta, et al., *A 2 per cent distance to  $z=0.35$  by reconstructing baryon acoustic oscillations - I. Methods and application to the Sloan Digital Sky Survey*, *Mon.Not.Roy.Astron.Soc.* **427** (2012), no. 3 2132–2145, [[arXiv:1202.0090](#)].
- [50] L. Anderson, E. Aubourg, S. Bailey, D. Bizyaev, M. Blanton, et al., *The clustering of galaxies in the SDSS-III Baryon Oscillation Spectroscopic Survey: Baryon Acoustic Oscillations in the Data Release 9 Spectroscopic Galaxy Sample*, *Mon.Not.Roy.Astron.Soc.* **427** (2013), no. 4 3435–3467, [[arXiv:1203.6594](#)].
- [51] C. Blake, E. Kazin, F. Beutler, T. Davis, D. Parkinson, et al., *The WiggleZ Dark Energy Survey: mapping the distance-redshift relation with baryon acoustic oscillations*, *Mon.Not.Roy.Astron.Soc.* **418** (2011) 1707–1724, [[arXiv:1108.2635](#)].
- [52] D. J. Eisenstein and W. Hu, *Baryonic features in the matter transfer function*, *Astrophys.J.* **496** (1998) 605, [[astro-ph/9709112](#)].
- [53] **WMAP** Collaboration, G. Hinshaw et al., *Nine-Year Wilkinson Microwave Anisotropy Probe (WMAP) Observations: Cosmological Parameter Results*, *Astrophys.J.Suppl.* **208** (2013) 19, [[arXiv:1212.5226](#)].
- [54] G. Mangano, G. Miele, S. Pastor, and M. Peloso, *A Precision calculation of the effective number of cosmological neutrinos*, *Phys. Lett.* **B534** (2002) 8–16, [[astro-ph/0111408](#)].
- [55] B. Follin, L. Knox, M. Millea, and Z. Pan, *First Detection of the Acoustic Oscillation Phase Shift Expected from the Cosmic Neutrino Background*, *Phys. Rev. Lett.* **115** (2015), no. 9 091301, [[arXiv:1503.07863](#)].